Simultaneous detection/separation of mineral dust and cirrus clouds using MODIS thermal infrared window data

R. A. Hansell,[1] S. C. Ou,[1] K. N. Liou,[1] J. K. Roskovensky,[2] S. C. Tsay,[3] C. Hsu,[3] and Q. Ji[4]

Received 17 January 2007; revised 14 March 2007; accepted 1 May 2007; published 9 June 2007.

[1] An integrated method for the simultaneous detection/separation of mineral dust and clouds for both daytime and nighttime conditions using MODIS thermal infrared window brightness temperature data has been developed. Based on the spectral variability of dust emissivity at 3.75, 8.6, 11 and 12 μm wavelengths, we combine three heritage approaches to identify dust and cirrus. MODIS data for three dust-laden scenes have been analyzed to demonstrate the effectiveness of this detection/separation method. The detected daytime dust and cloud coverage for the Persian Gulf case compares reasonably well to those from the "Deep Blue" algorithm developed at NASA-GSFC. Validation of the nighttime dust and cloud detection method has been carried out by using the cases surrounding Cape Verde and Niger, West Africa, on the basis of the coincident and collocated ground-based micro-pulse lidar measurements.
Citation: Hansell, R. A., S. C. Ou, K. N. Liou, J. K. Roskovensky, S. C. Tsay, C. Hsu, and Q. Ji (2007), Simultaneous detection/separation of mineral dust and cirrus clouds using MODIS thermal infrared window data, *Geophys. Res. Lett.*, *34*, L11808, doi:10.1029/2007GL029388.

1. Introduction

[2] Global detection of tropospheric mineral dust is often hampered by the radiative effects of clouds, in particular thin cirrus [*Roskovensky and Liou*, 2005]. The effects of not properly detecting dust outbreaks may result in (1) large biases in satellite retrieved cloud and surface parameters [*Reid et al.*, 2003b], (2) impeding military [*Miller*, 2003] and commercial operations due to severe reduction of near-surface visibility, and (3) causing adverse health effects [*Prospero*, 1999].

[3] Recently, a number of visible and IR channel techniques have been developed for dust detection. *Hutchison and Jackson* [2003] showed that the reflection by sand increases steadily with wavelength in the 0.4 to 1.0 μm spectral region and implemented a 0.41 μm threshold test to identify clouds over desert surfaces in the future NPOESS/VIIRS cloud mask. *Miller* [2003] implemented a multi-spectral dust enhancement algorithm that combines dust coloration properties with the MODIS negative 11–12 μm brightness temperature difference (*BTD*11-12) for the daytime and nighttime detection of dust particles over dark and bright surfaces. *Roskovensky and Liou* [2005] followed the conceptual approach of Hutchison and Jackson and used a dust detection parameter in conjunction with the cirrus detection parameter [*Roskovensky and Liou*, 2003] to separately identify thin cirrus clouds from airborne dust.

[4] This paper focuses on the detection of dust over major dust outbreak and transport areas using MODIS infrared brightness temperatures (*BT*). We have developed an integrated approach to simultaneously detect and separate airborne mineral dust from clouds along with distinguishing cloud phase to facilitate dust aerosol remote sensing, with emphasis on nighttime dust events. This approach is based on the spectral variability of dust emissivity at 3.75, 8.6, 11 and 12 μm wavelengths. MODIS data for three dust-laden scenes, including a daytime dust case over the Persian Gulf and two nighttime dust events over the Cape Verde Islands and Niger, West Africa, have been analyzed to demonstrate the effectiveness of this approach. The organization of this paper is as follows. Section 2 discusses the dust detection methodology. Section 3 presents the MODIS data and details of each case study. Finally, a summary along with potential applications is given in section 4.

2. Dust Detection Methodology

[5] The integrated dust detection (IDD) technique consists of three independent approaches described below. The first is a threshold detection technique referred to as the "*D* (dust) –parameter method" following the concept developed by *Roskovensky and Liou* [2005]. The *D*-parameter is defined as

$$D = exp\{[(rr)a + (BTD11 - 12) - b]\}, \quad (1)$$

where *rr* represents the 0.54 μm/0.86 μm reflectance ratio, *a* is a scaling factor, and *b* is the *BTD*11-12 offset. Roskovensky and Liou showed that the *D*-parameter is highly sensitive to cirrus cloud optical depth, since it is an exponential function of *rr* and *BTD*11-12. Because the *D*-parameter test requires solar channel data, it can only be applied to local daytime conditions. To detect nighttime dust, we have devised a *D**-parameter test in terms of *BTD*11-12 and *BTD*8-11 (the *BTD* between 8.6 μm and 11 μm) as follows:

$$D^* = exp\{[(BTD11 - 12) - C]/[(BTD8 - 11) - E)]\}, \quad (2)$$

[1]Department of Atmospheric and Oceanic Sciences, University of California, Los Angeles, California, USA.
[2]Sandia National Laboratories, Albuquerque, New Mexico, USA.
[3]NASA Goddard Space Flight Center, Greenbelt, Maryland, USA.
[4]Earth System Science Interdisciplinary Center, University of Maryland at College Park, College Park, Maryland, USA.

0094-8276/07/2007GL029388$05.00

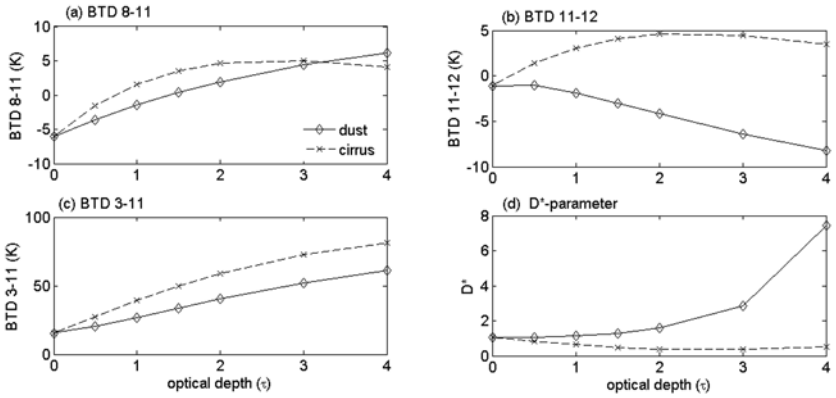

Figure 1. Simulations of the *BTD* and *D**-parameter versus optical depth (τ) for dust (pure quartz) and cirrus over land surface whose soil composition is prescribed to be quartz. Solar and satellite zenith angles used were 30° and 0°, respectively. (a) *BTD*8-11, (b) *BTD*11-12, (c) *BTD*3-11, and (d) *D**-parameter.

where parameters C and E are the thermal offsets for *BTD*11-12 and *BTD*8-11, respectively. These offsets are adjustable based on analyses of dust-laden MODIS scenes and simulations to enhance the dust signal against a cloud-filled background. In comparison to the *D*-parameter test, the *BTD*8-11 term replaces the reflective ratio *rr*, providing an additional constraint on dust detection. This is significant since many silicate minerals that have strong restrahlen bands often absorb more at 8.6 μm than at 11 μm, leading to a negative *BTD*8-11. In contrast, cirrus cloud (ice) particles absorb more at 11 μm than at 8.6 μm, producing a positive *BTD*8-11, except when there is a large amount of water vapor, which could make *BTD*8-11 negative due to the enhanced water vapor absorption at 8.6 μm.

[6] The detection test is so designed that $D^* > 1$ indicates dust and $D^* \leq 1$ indicates cloud. This method is herein referred to as dust filter 1 (DF1). DF1 does not discriminate cloud phase, however. Theoretical calculations similar to those conducted by Roskovensky and Liou have been performed to evaluate the *BTD* terms in equation (2) for the four IR channels as a function of dust and cloud optical depths. The *BTD*s for both cirrus/water clouds and various compositions of dust including quartz, quartz mixed with hematite, and several clays have subsequently been analyzed.

[7] Figures 1a, 1b, and 1d show the calculated *BTD*8-11, *BTD*11-12, and *D**-parameter as functions of optical depth for cirrus and dust conditions over land. The dust was assumed to be pure quartz with a spherical shape, and its optical properties were generated from a Lorenz-Mie scattering code based on the spectral refractive indices given by *Shettle and Fenn* [1979]. Cirrus clouds were modeled following the approach developed by *Roskovensky and Liou* [2005]. A typical Persian Gulf summer atmospheric profile was used and the land surface reflectivity was modeled by using the JPL Advanced Spaceborne Thermal Emission and Reflection Radiometer (ASTER) spectral library, assuming a dark brown quartz surface. For the computation of *D**, the offsets C and E in equation (2) were set as -0.5 and 15, respectively, based on prior analyses of MODIS dust-laden scenes and simulations. Theoretical simulations suggest that offset C can vary between -0.5 and 0.35, as *BTD*11-12 is sensitive to dust composition, surface type, and column water vapor. Further work is required to develop a dynamical adjustment to these offsets. However, for the purposes of this study, the chosen constant values are sufficient to demonstrate the effectiveness of the present approach.

[8] For dust, *D** increases exponentially with optical depth (τ_d) due to a large negative *BTD*11-12 (Figure 1b). Because of this strong sensitivity, the *D** test using the prescribed model parameters is shown to be effective in separating dust from cirrus and thus appears to be an excellent initial approach for detecting dust.

[9] Sensitivity tests were performed to evaluate the *D**-parameter's response to changes in dust layer height, particle asphericity, low clouds and other aerosol. For dust layer height, theoretical simulations suggest that increasing the altitude decreases the *D**-parameter's sensitivity, because an increase in thermal emission from a vertically extended dust layer tends to increase *BTD*11-12. For particle asphericity, we chose oblate spheroids with aspect ratios of 2 and 3, consistent with previous research results [*Reid et al.*, 2003a]. The *D**-parameter was found to be slightly larger than that over the spherical value on the order of 0.5–1% due to an increase in *BTD* 8-11 by ~1K. For spheroids, particle asphericity effects are minimal. For low clouds, theoretical simulations over a quartz surface indicate that day/nighttime coarse-mode dust will not be detected when it is located beneath a cloud layer of moderate optical depth ($\tau_{cld} \sim 4$). Elevated dust above clouds, however, particularly at night, can be detected provided the dust has a minimum optical depth ($\tau_d \geq 0.07$). Lastly, dust was replaced by other aerosol: coarse-mode sea-salt (RH = 80%), ammonium sulfate and black carbon in cloud-free conditions. For the cases tested, the *D**-parameter fell below the threshold ($D^* < \varepsilon$) where $\varepsilon = 1$ using the prescribed thermal offsets in equation (2). Adjustment of these offsets could potentially be used to separate dust from these other aerosol in cloud-free conditions.

[10] The second approach is the *BTD*8-11 vs. *BTD*11-12 slope method, which follows the principle of the cloud phase algorithm developed by *Strabala et al.* [1994]. We modified this algorithm and used the slope of the best-fit straight line for the scatter plot of *BTD*8-11 vs. *BTD*11-12 to identify dust and cloud. Specifically, if a grid domain contains less than a prescribed number of clear pixels, using the MODIS cloud mask (MOD-35, Level 2), then both *BTD*8-11 and *BTD*11-12 are calculated, a linear regression is performed, and the slope of the best-fit line (i.e., Δ*BTD*8-

11/Δ*BTD*11-12 where Δ denotes a differential change of the parameter) is determined. If the slope is negative, the domain pixels are identified as dust. Scatter data plots over the dust-filled regions from selected MODIS scenes and radiative transfer simulations show that the slope is negative for dust. Similar to cirrus clouds, although of opposite sign, the change in *BTD*8-11 is much larger than the corresponding change in *BTD*11-12, which follows from the differences in the spectral absorption coefficients for common dust minerals. If the slope is positive, however, the pixels are flagged as cloud. For the identified cloudy pixels, if the slope is between 0 and 1, the domain pixels are flagged as water cloud based on thresholds established from a sample of observed cases. Otherwise, the domain pixels are labeled as cirrus cloud (for slope greater than 1). This test is referred to as dust filter 2 (DF2). It takes the output of DF1 which initially identifies the dust, and then applies the slope test to confirm the presence of dust. If both *D**-parameter and *BTD* slope tests identify a pixel as dust, it is classified as dust, otherwise it is classified as cloud and its thermodynamic phase is subsequently determined.

[11] The third approach is the *BTD*3-11 (*BTD* between 3.75 μm and 11 μm) method. Based on limited observations and model simulations, data points of *BTD*3-11 vs. the 11 μm *BT* fall into: separate clusters for clear-sky, dust, and water and cirrus clouds. For the same 11 μm *BT, BTD*3-11 for cirrus clouds generally exhibit the largest values due to a significant difference in water vapor and cloud spectral optical properties for the two bands. The *BTD*3-11 for dust and water cloud is smaller than that for cirrus due to less variation in their spectral optical properties. Thus, dust and cirrus cloud can be separated based on the differences in *BTD*3-11. This method is quite sensitive to the assumed dust composition and surface parameters as well as column water vapor. Figure 1c shows that *BTD*3-11 for dust is a function of the dust optical depth (τ_d). This dependency can be further used to qualitatively separate optically thin ($\tau_d < 1$) and thick ($\tau_d > 1$) dust regions, which are identified by DF1 and DF2 tests, while detection thresholds can be established on the basis of simulations and observational data.

3. Data and Case Studies

[12] Three MODIS dust scenes were selected to demonstrate the effectiveness of the IDD approach presented above. The MOD-35 cloud mask was used in the current approach to identify clear pixels based on the 99% confidence flag. This forms the basis for our detection analysis since the algorithm is applied where the MOD-35 flags clouds. A 1 km land/water mask was also employed to define land and ocean surfaces. A data reduction method subdivides the MODIS granule into 5 $\times$ 5 grids covering an area of approximately 25 km^2. If MOD-35 identifies at least 75% clear sky pixels in the grid space it is labeled as clear, otherwise the algorithm proceeds to the *BTD* tests. Using the central frequency of each channel, the measured radiances are converted to equivalent *BT*.

[13] The first case is a daytime MODIS/Aqua overpass across the Persian Gulf on September 12, 2004 at 1005UTC. The MODIS visible image shown in Figure 2a is provided for reference. The detection results (Figure 2b) capture a large dust outbreak area (white circle), transported over the northern Persian Gulf and along the Strait of Hormuz. The MODIS cloud mask product indicates that clear sky is predominant over most of the land areas. Consequently, there is almost no detected dust over land, although uncertainties in the cloud mask may lend itself towards detecting optically thin dust over land surfaces, denoted by the light gray color shown in Figure 2b. Dust detection over seas, on the other hand, is quite apparent. Figure 2b shows that the present integrated approach detects dust (red/yellow) over the northern Persian Gulf, the Strait of Hormuz, and the Gulf of Oman. Light to moderate dust loadings ($\tau_d < 1$) shown in red were found to occupy about 42% of the area over water. Likewise, about 2% of the area (yellow) was found to contain high dust loads ($\tau_d > 1$). Clusters of water clouds (green) are seen over the Strait of Hormuz, the Gulf of Oman and over portions of the Oman mountain range. Qualitative comparisons of the spatial coverage of our detected clouds with those in the visible image and the MODIS cloud/phase mask (MOD-06, Level 2) shows reasonable agreement. Note the clouds in Figure 2a have more structure compared to dust which helps further distinguish between the two fields particularly around the Strait of Hormuz. Our detected dust complements the MOD-06 water clouds identified over the Persian Gulf since this region was heavily obscured by dust. This is evident in the Deep Blue results (Figure 2c) which show substantial dust coverage. Scattered cirrus clouds (blue) were found over parts of the dust plume in the Persian Gulf. Although the visible MODIS image shows evidence for clouds in this region, some may actually be due to dust where the *D**-parameter falls below its threshold due to a positive increase in *BTD*11-12. This can be attributed to changes in mineral composition, surface type and water vapor amounts. For example, the clay, illite, can cause the D*-parameter to fall below its threshold making it necessary to adjust thermal offset C.

[14] Figure 2c shows the contours of the retrieved dust optical depth at $\lambda = 0.50$ μm for the same date presented by *Hsu et al.* [2004] using a daytime solar algorithm, referred to as Deep Blue. For details of the Deep Blue algorithm, please refer to *Hsu et al.* [2004]. Comparing Figure 2b to Figure 2c shows our integrated approach produces similar dust coverage, particularly for the regions over the Persian Gulf. In Figure 2c, for example, the results from Deep Blue capture the dust outbreak at the northern tip of the Persian Gulf (white circle) and a significant dust loading found along the Strait of Hormuz. The white patches indicate areas of clouds where no retrieval was performed. Our integrated approach also detects clouds near to those of Deep Blue, particularly along southern Iran's coastal regions. The retrieved optical depths ($\lambda = 0.50$ μm) at the AERONET Sir-Bu-Nuair site (25°N, 54°E; within the white square), collocated and coincident with the Aqua overpass, were found to be about 1.018. For the same area, the Deep Blue retrieved τ_d was about 1.20, while the integrated approach identifies the dust region as optically thin with an estimated τ_d close to 1 in close agreement with those from Deep Blue and AERONET. The integrated approach can also be useful in the sun-glint area by employing only DF1 and DF2 since *BTD*8-11 and *BTD*11-12 are not subject to variations in solar reflection. This capability in the current approach could complement MODIS daytime dust detection algorithms.

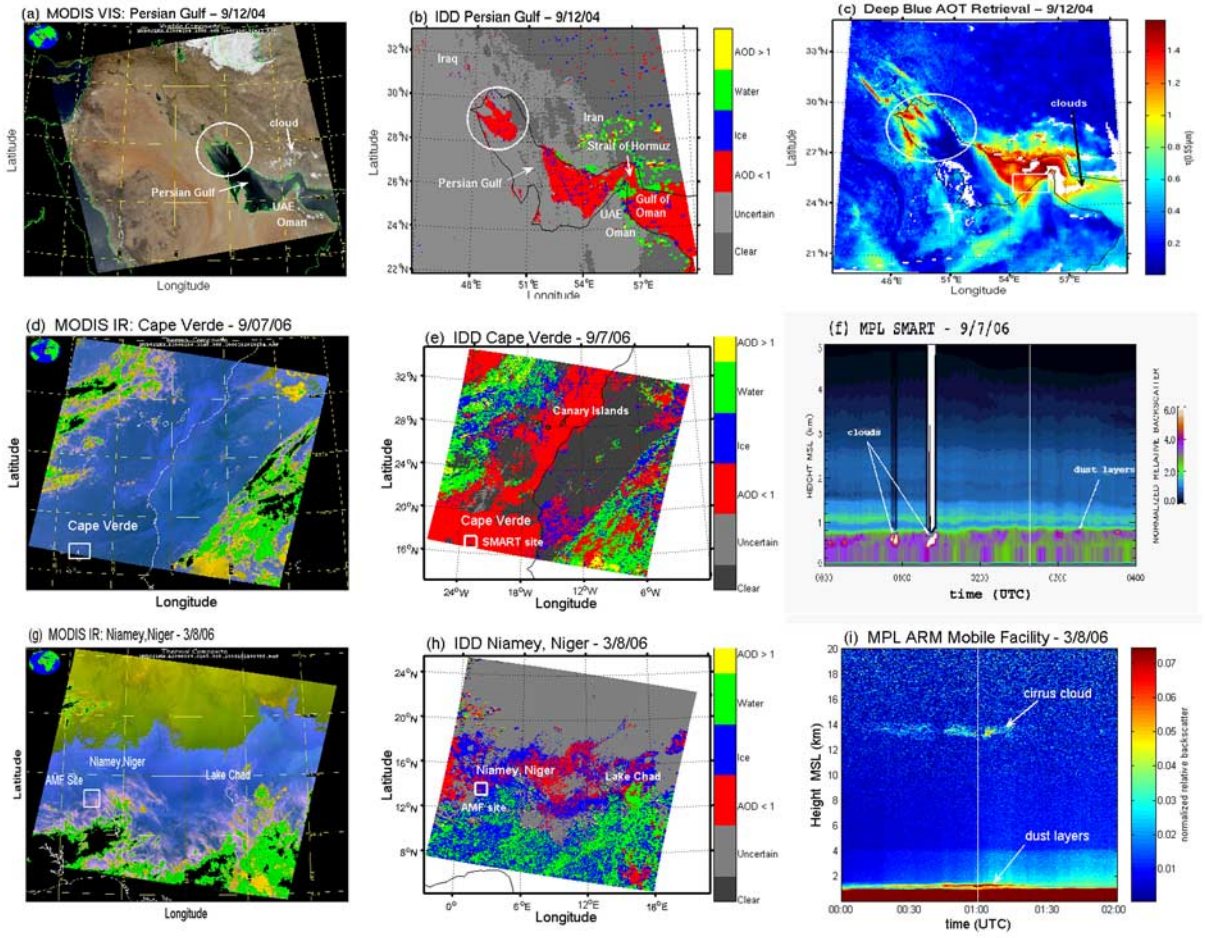

Figure 2. (a) MODIS visible image of the Persian Gulf on September 12, 2004, at 1005UTC. (b) Daytime IDD over the Persian Gulf. (c) Retrieved visible optical depths using the Deep Blue scheme over the Persian Gulf. (d) MODIS IR image showing the Cape Verde Islands on September 7, 2006, at 0245UTC. (e) Nighttime IDD over the Cape Verde Islands. (f) MPL (SMART) normalized backscatter at Sal on the Cape Verde Islands during NAMMA. (g) MODIS IR image showing Niamey, Niger, on March 8, 2006, at 0100UTC. (h) Same as Figure 2e, except over Niamey, Niger. (i) MPL (AMF) normalized backscatter at Niamey.

[15] The second case chosen is associated with a nighttime dust scene over the Cape Verde Islands during the recent NASA African Monsoon Multidisciplinary Analysis (NAMMA) field campaign on September 7, 2006 at 0245UTC. The MODIS IR image shown in Figure 2d is provided for reference. The white box at the bottom of Figure 2e shows the location of the islands at 16.732°N, 22.935°W. Evident in this scene is a prominent dust plume with small to moderate optical depths (red) that follows the African coastline. The division of dust along the coastline further illustrates the difficulties with over land detection. As in the previous case, MOD-35 indicates clear sky over most of the land areas, so very little dust is detected over land leading to the coastal divisions. Much of the area including Sal Island is labeled 'uncertain' (gray), to account for uncertainties in the MOD-35. There also appears to be a continental outflow of dust (red) around 18°N, 15°W, near Mauritania and the Western Sahara, both of which are major dust source regions. Further inland, streaks of optically thicker dust (yellow) are found. Along the northwest and southeast corners of the MODIS granule are bands of mostly water clouds mixed with some cirrus. Validating cloud phase away from surface sites proves difficult due to the lack of data; however we suspect on the basis of the current approach that clouds occupied these areas with slopes indicative of both water and ice. It is clear more cases are needed to have a complete validation, however this approach demonstrates a clear potential for dust and cloud separation during nighttime conditions.

[16] The Surface-sensing Measurements for Atmospheric Radiative Transfer and Chemical Optical and Microphysical Measurements for in situ Troposphere (SMART-COMMIT) developed at Goddard Space Flight Center/NASA was deployed at the Sal Island during NAMMA. SMART operated a NASA Micro-Pulse Lidar Network instrument (MPL) [*Welton et al.*, 2001], a key instrument for profiling the vertical structure of aerosol and clouds, which operated continuously, with the exception of local noon. Figure 2f shows the MPL-network Level 1.0 normalized relative backscatter (NRB) product, described by *Campbell et al.* [2002], for September 7, 2006.

[17] At the Aqua overpass time (0245UTC) marked by the solid white line, a strong dust aerosol signature up to 4 km is evident. This is likely associated with the Saharan

air layer transport, similar to the lidar observations presented by *Sassen et al.* [2003]. Almost two hours before the Aqua overpass, low level clouds around 1 km were detected. Our current detection scheme for the dust layer over the Sal Island is consistent with the MPL observations. In addition, coincident measurements from the SMART's AERI instrument observed higher brightness temperatures of about 5 K at the 10 μm wavelength, where dust aerosol absorbs more IR radiation than other wavelengths in the window region.

[18] In addition to the preceding two cases, we have selected another nighttime dust scene over Niamey, Niger in West Africa, observed by the ARM Mobile Facility (AMF) on March 8, 2006 at 0100UTC. The MODIS IR image shown in Figure 2g is provided for reference. The AMF experienced a significant dust episode, beginning on March 7, 2006 and lasted several days. The white box in Figure 2h marks the location of AMF at 13.477°N, 2.175°E. Satellite images indicate that the dust storm originated in the central Sahara (Niamey News, ARM website). The detection results in Figure 2h show a prominent dust band with light to moderate optical depths (red) traversing the north central parts of the continent, particularly through Niger and Chad. A significant amount of cirrus clouds (blue) was also found over the detected dust, with an extensive mix of both water (green) and cirrus clouds to the south. An MPL has been continuously operating at the AMF since November 2005. Figure 2i shows the instrumentally corrected NRB signal for March 8, 2006. At the MODIS/Aqua overpass time (0100UTC), marked by the solid white line, a significant amount of dust aerosol can be seen up to 4 km, including a high-level cirrus cloud at 13 km. Again, the present scheme has the capability to detect dust directly over the AMF site and to identify overlying cirrus clouds consistent with the MPL observations.

4. Summary

[19] An integrated method for the detection and separation of mineral dust from cirrus clouds using the MODIS thermal IR window band data has been presented. We combined the D^*-parameter, *BTD* slope, and *BTD*3-11 methods to detect dust and cirrus for both nighttime and daytime scenes. This integrated approach was applied to three MODIS dust cases to demonstrate its feasibility and reliability. The first is a daytime case over the Persian Gulf. By comparing the results determined from the integrated method and the NASA Deep Blue solar retrieval algorithm, we demonstrated the reliability of the present approach in detecting dust events during daytime. The two other cases are nighttime scenes over the Cape Verde Islands and Niamey, Niger. By comparing the detection results to the MPL observations at each site, we illustrated that the present scheme can be used to detect dust and to separate dust from cirrus during nighttime conditions with some confidence. Of course, more cases are needed to have a complete validation of the present approach. Nevertheless, it offers a variety of promising applications, including: (1) scene classification for the dust radiative forcing studies, (2) dust aerosol correction for improved sea surface temperature retrievals and dust data assimilation in the coupled ocean-atmosphere model, (3) application of the detection results to the current operational daytime aerosol retrieval algorithm, and (4) assessment of the nighttime dust hazard to improve transportation safety and mitigate dust's adverse health effects.

[20] **Acknowledgments.** The MODIS cloud-mask read algorithm from S. Nasari/S.W. Seemann 2001 (CIMSS/SSEC) was used in this study and the MODIS data and images were obtained from the NASA LAADS Web site. The NAMMA MPL data was acquired through the NASA Micro-Pulse Lidar Network which is funded by the NASA Earth Observing System and Radiation Sciences Program. Sun-photometer data from the Sir-Bu-Nuair site was provided by the NASA AERONET Program. The AMF MPL data was acquired through the ARM data archive. We are grateful to the following people: J. Campbell for producing the NAMMA MPL plot, R. Coulter for help with the AMF MPL data correction, and to C. Zender and T. Roush for making available the mineral datasets. We are also grateful to the reviewers of this manuscript for their helpful and insightful comments. This research was supported by NASA grants NNC5-712 and NNG04GG91G.

References

Campbell, J. R., D. L. Hlavka, E. J. Welton, C. J. Flynn, D. D. Turner, J. D. Spinhirne, V. S. Scott, and I. H. Hwang (2002), Full-time, eye-safe cloud and aerosol lidar observation at Atmospheric Radiation Measurement program sites: Instruments and data analysis, *J. Atmos. Oceanic Technol.*, *19*, 431–442.

Hsu, N. C., S. C. Tsay, M. D. King, and J. R. Herman (2004), Aerosol properties over bright-reflecting source regions, *IEEE Trans. Geosci. Remote Sens.*, *42*, 557–569.

Hutchison, K. D., and J. M. Jackson (2003), Cloud detection over desert regions using the 412 nanometer MODIS channel, *Geophys. Res. Lett.*, *30*(23), 2187, doi:10.1029/2003GL018446.

Miller, S. D. (2003), A consolidated technique for enhancing desert dust storms with MODIS, *Geophys. Res. Lett.*, *30*(20), 2071, doi:10.1029/2003GL018279.

Prospero, J. M. (1999), Long-range transport of mineral dust in the global atmosphere: Impact of African dust on the environment of the south eastern United States, *Proc. Natl. Acad. Sci. U. S. A.*, *96*, 3396–3403.

Reid, E. A., J. S. Reid, M. M. Meier, M. R. Dunlap, S. S. Cliff, A. Broumas, K. Perry, and H. Maring (2003a), Characterization of African dust transported to Puerto Rico by individual particle and size segregated bulk analysis, *J. Geophys. Res.*, *108*(D19), 8591, doi:10.1029/2002JD002935.

Reid, J. S., et al. (2003b), Analysis of measurements of Saharan dust by airborne and ground-based remote sensing methods during the Puerto Rico Dust Experiment (PRIDE), *J. Geophys. Res.*, *108*(D19), 8586, doi:10.1029/2002JD002493.

Roskovensky, J. K., and K. N. Liou (2003), Detection of thin cirrus from 1.38 μm/0.65 μm reflectance ratio combined with 8.6–11 μm brightness temperature difference, *Geophys. Res. Lett.*, *30*(19), 1985, doi:10.1029/2003GL018135.

Roskovensky, J. K., and K. N. Liou (2005), Differentiating airborne dust from cirrus clouds using MODIS data, *Geophys. Res. Lett.*, *32*, L12809, doi:10.1029/2005GL022798.

Sassen, K., P. J. DeMott, J. M. Prospero, and M. R. Poellot (2003), Saharan dust storms and indirect aerosol effects on clouds: CRYSTAL-FACE results, *Geophys. Res. Lett.*, *30*(12), 1633, doi:10.1029/2003GL017371.

Shettle, E. P., and R. W. Fenn (1979), Models for the aerosols of the lower atmosphere and the effects of the humidity variations on their optical properties, *Environ. Res. Pap. 675*, 94 pp., Air Force Geophys. Lab., Hanscom AFB, Mass.

Strabala, K. I., S. A. Ackerman, and W. P. Menzel (1994), Cloud properties inferred from 8–12 μm data, *J. Appl. Meteorol.*, *33*, 212–229.

Welton, E. J., J. R. Campbell, J. D. Spinhirne, and V. S. Scott (2001), Global monitoring of clouds and aerosols using a network of micro-pulse lidar systems, *Proc. Int. Soc. Opt. Eng.*, *4153*, 151–158.

R. A. Hansell, K. N. Liou, and S. C. Ou, Department of Atmospheric and Oceanic Sciences, University of California, Los Angeles, Los Angeles, CA 90095-1565, USA. (rhansell@atmos.ucla.edu)

C. Hsu and S. C. Tsay, NASA Goddard Space Flight Center, Code 613.2, Greenbelt, MD 20771, USA.

Q. Ji, Earth System Science Interdisciplinary Center, University of Maryland at College Park, 2207 Computer and Space Sciences Building #224, College Park, MD 20742-2465, USA.

J. K. Roskovensky, Sandia National Laboratories, Mail Stop 0406, Albuquerque, NM 87185, USA.